Online MTPTA and MTPIA Control of Brushless Doubly Fed Induction Motor Drives

Hamidreza Mosaddegh Hesar, Hossein Abootorabi Zarchi, and Gholamreza Arab Markadeh

***Abstract*—This article proposes a nonlinear controller for brushless doubly-fed induction motor (BDFIM) drives on the basis of input–output feedback linearization (IOFL). In the proposed control approach, first, the maximum torque per inverter ampere (MTPIA) control strategy is considered by applying a fifth-order (reduced-order) model of BDFIM. By realizing the MTPIA, the control winding (CW) current magnitude is minimized under the constraint of constant torque. The realization criterion of MTPIA approach is independent of torque level and CW frequency. To fairly share the current between stator windings and minimizing the total current magnitude for a given torque, the MTPIA idea should be extended. Since, the power winding (PW) of BDFIM is not controllable, obtaining this purpose is a challenge. Therefore, to solve this problem, the model-based maximum torque per total ampere (MTPTA) control is introduced for BDFIM drives and the conditions for realizing this strategy are determined. It should be noted that the total amperes refer to the sum of the PW and the CW current magnitudes. In addition, using the fifth-order model of BDFIM, a nonlinear controller is developed based on IOFL technique which is capable to force the deviation from realization criterion of both proposed strategies to zero while the torque is controlled with high accuracy. The overall stability of the proposed controller is proven using the Lyapunov control theory. The validity of the proposed approach is finally verified by simulation and experimental results.**

***Index Terms*—Brushless doubly fed induction motor (BDFIM), control winding angle, fifth-order model, input-output feedback linearization (IOFL), maximum torque per total ampere (MTPTA).**

NOMENCLATURE

$\vec{V}$, $\vec{I}$, $\vec{\psi}$	Voltage, current, flux vectors.
T_e	Electromagnetic torque.
R	Winding resistance.
L_l	Leakage inductance.
L_{1r}, L_{2r}	Coupling inductances between stator windings and rotor.
p	Pole pair number.
N_r	Number of nests.
ω_1, ω_2	Angular speed.
s	Slip.
θ	Current angle.
f	Frequency.
Subscripts	
$1, 2, r$	PW, CW, and rotor.
d, q	Rotating frame axis.
α, β	Stationary frame axis.

Manuscript received September 26, 2019; revised January 29, 2020 and March 27, 2020; accepted May 19, 2020. Date of publication June 3, 2020; date of current version September 4, 2020. Recommended for publication by Associate Editor L. Dalessandro. *(Corresponding author: Hossein Abootorabi Zarchi.)*

Hamidreza Mosaddegh Hesar and Hossein Abootorabi Zarchi are with the Department of the Electrical Engineering Faculty of Engineering, Ferdowsi University of Mashhad, Mashhad 9177948974, Iran (e-mail: hamid.mosaddegh@mail.um.ac.ir; abootorabi@um.ac.ir).

Gholamreza Arab Markadeh is with the Department of Engineering, Shahrkord University, Shahrekord 8818634141, Iran (e-mail: arab-gh@eng.sku.ac.ir).

Color versions of one or more of the figures in this article are available online at https://ieeexplore.ieee.org.

Digital Object Identifier 10.1109/TPEL.2020.3000150

I. Introduction

BRUSHLESS doubly-fed induction machines (BDFIMs) have been shown promising prospect as a potential alternative to the existing commercial solutions. In generator mode, the BDFIM (which is also known as a self-cascaded machine) is considered to be an emerging competitor for older structures, such as squirrel cage induction generator, doubly-fed induction generator, and permanent magnet synchronous generator, due to its unique specifications. In the field of adjustable speed drives (ASDs), the first efforts in research and development of BDFIM, were carried out in Kanazawa institute of technology, Japan, and Oregon state university, USA, early in the 1990s [1]. Meanwhile, the capabilities of BDFIM for using in ASDs were investigated by A. K. Wallace. The laboratory results confirmed the benefits of BDFIM compared to the conventional drives. The ability of this machine has been investigated for wind turbine applications [2], [3], industrial drives [4], [5], and small hydro plants [6], as well as supplying power to ships [7].

A multitude of high performance techniques of BDFIM drives including field oriented control (FOC) and direct torque control have been proposed [8]–[10], so far. The control of BDFIM constitutes a theoretically challenging problem, due to its inherent nonlinear dynamics. To achieve the better dynamic performance of BDFIM, FOC is a proper option that ensures independent torque and flux control. The proportional-integral (PI) based FOC approach partially linearizes the BDFIM drive by controlling it in a frame which rotates with the power winding (PW) flux vector. To entirely linearize and decouple the BDFIM model, this control scheme can be upgraded by implementing a nonlinear controller such as input-output feedback linearization (IOFL). The IOFL is a nonlinear control technique that its main idea is to transform an inherently nonlinear plant into an equivalent linear plant. As a result, a linear controller is designed for linear plant and then it is possible to determine the control inputs using the decoupling matrix [11]. However, the IOFL control conventionally suffers from internal dynamics which cannot be often proven to be stable under the transient and

steady-state conditions. This means that the control system will be only locally stable if the controller gains are properly adjusted. As a result, the Lyapunov-based IOFL control is proposed in this article for BDFIM drives to analytically proven the total stability of the controller.

In the last few decades, an extensive amount of research on the subject of energy saving standing on maximum torque per ampere (MTPA) based control technique has been considered for singly-fed ac motor drives [12]–[15]. However, a few research has been published with the aim of efficiency improvement of doubly-fed motor drives in general and implementation of MTPA strategy in particular. One of them given in [16] deals with steady-state efficiency optimization of BDFIM based on an offline search algorithm (look-up table approach). Theoretical analysis of some of the important control properties of the ideal brushless doubly-fed reluctance machine (BDFRM), including maximum torque per total ampere (MTPTA), has been proposed by Betz and Jovanovic [17]. For singly-fed machines which are fully controllable, the implementation of the MTPA control strategy is routine and it has not any complexity. To do this, the stator current is minimized for a given torque by model or search-based approaches. For doubly-fed machines, the minimization of total stator current magnitudes is not however straightforward by a fractionally rated frequency converter. A search-based MTPTA control strategy has been introduced in [18], for simulated BDFIM drive. It is shown that by tracking the power winding (CW) *d*-axis current as reference signal, the proposed strategy is realized.

This article will attempt to present a theoretical approach for realization of model-based MTPTA strategy, as one of the most important control property of BDFIM. In this regard, using the CW current angles which are mathematically approximated by an appropriate curve, the minimum value of total current magnitude is determined for each given torque. The proposed strategy preserves all benefits of model-based control approaches such as fast response and high accuracy. The other contributions of this article are highlighted as follows.

1) The parameter-free maximum torque per inverter ampere (MTPIA) control strategy is applied and it is proven to have the minimum inverter rating, the CW *d*-axis current should be kept at zero $(i_{2d} = 0)$. It is worth noting that the realization criterion of MTPIA strategy is independent of the torque level and CW frequency.
2) In order to enhance the performance of BDFIM drives, a nonlinear control technique is developed based on IOFL theory. Consequently, the control inputs are chosen so that the Lyapunov function candidate satisfies the stability criterion. Later, in this article, the detailed description of the nonlinear controller will be presented.

In this article, to overcome the complexities of the complete model of BDFIM caused by the rotor state variables, a fifth-order model of BDFIM is used which facilitates the control approach implementation without loss of accuracy. This model formed by ignoring the contribution of direct cross couplings is a much better approximation to represent the complete model of BDFIM compared to the core model derived only for analyzing the BDFIM performance [19]. The core model is an oversimplified version of the equivalent circuit of BDFIM obtained by omitting the magnetizing reactances and the stator and the rotor resistances [20]. Considering the fifth-order model, the BDFIM model turns into a conventional doubly-fed induction machine (DFIM), and consequently the BDFIM can be modeled and controlled similar to DFIM.

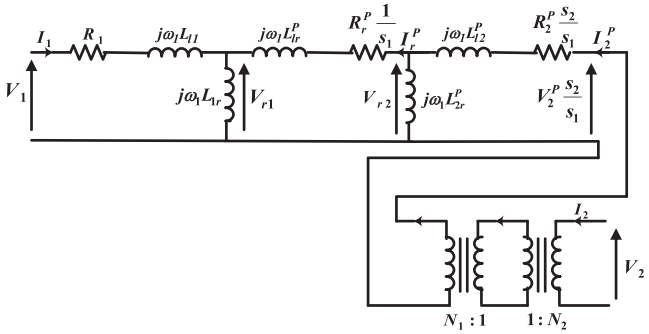

Fig. 1. Steady-state equivalent circuit of BDFIM.

The rest of this article is organized as follows. In Section II, the fundamental of BDFIM and method for its model order reduction are discussed. Section III presents the MTPIA and MTPTA strategies principles. The IOFL nonlinear controller is developed for BDFIM in Section IV. In Section V, the simulation and experimental results are evaluated. Finally, Section VI concludes the article.

II. Fundamental of BDFIM and Modeling

The BDFIM is a single frame and brushless machine which has two sinusoidally distributed stator windings, i.e., the PW and the CW. The PW has p_1 pole pair directly connected to the grid and the CW has p_2 pole pair supplied by variable frequency converter with less capability than the BDFIM (synchronous mode). To avoid direct coupling, it is essential that the two stator windings have different number of pole pairs [21]. There are two distinct modes of operation; the induction mode (simple induction and cascade induction) and the synchronous mode. The most attractive mode of operation is synchronous mode. In this mode, due to the indirect coupling effect, the frequencies of the rotor currents induced by the two counter-rotating fields of the two stator windings become identical [22]. This constraint leads to the so-called synchronous rotor speed

$$\omega_r = \frac{\omega_1 + \omega_2}{p_1 + p_2}. \tag{1}$$

When the PW excitation is at grid frequency and the CW excitation is at zero frequency, the natural synchronous speed will achieve. Equation (1) indicates that the BDFIM rotor speed can be controlled by adjusting the CW frequency. In other words, the synchronous rotor speed is independent of the load torque unless a severe disturbance occurs [23]. The slips for the two stator windings are defined as

$$s_i \triangleq \frac{\omega_i/p_i - \omega_r}{\omega_i/p_i} = \frac{\omega_i - p_i\omega_r}{\omega_i} \quad i = 1, 2. \tag{2}$$

The steady-state equivalent circuit of BDFIM has been depicted in Fig. 1. This circuit is valid for all operation modes of BDFIM including synchronous mode. In this mode, the BDFIM

TABLE I
BDFIM PARAMETERS

Parameter	Value	Parameter	Value
PW pole-pair	2	R_1 (Ω)	1.3012
CW pole-pair	4	R_2 (Ω)	3.7171
PW rated voltage (V)	180 (at 50 Hz)	R_r (Ω)	1.1237
CW rated voltage (V)	180 (at 50 Hz)	L_{lr} (H)	0.1863
PW rated current (A)	10	L_{2r} (H)	0.0998
CW rated current (A)	4.5	L_{l1} (H)	0.0047
Rated torque (N.m)	20	L_{l2} (H)	0.0053
Natural speed (rpm)	500	L_{lr} (H)	0.0206

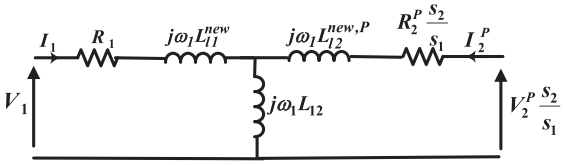

Fig. 2. Steady-state equivalent circuit of BDFIM for fifth-order model.

consists of three torque components. The first component is the synchronous torque which exists due to the indirect coupling of two stator windings magnetic fields. The other two components are asynchronous torques composed by direct cross-coupling of the PW and the rotor (first induction machine), as well as the CW and the rotor (second induction machine). The couplings between stator and rotor fields are poorer than the indirect cross-coupling between stator fields, hence the induction machines are negligible [20]. The asynchronous torque components are caused by R_r/s similar to the conventional induction machine. By varying the rotor speed in the range of $\pm 30\%$ around the natural speed, the rotor slips due to the magnetic fields of the PW (s_1) and the CW (s_2) are high. For instance, for the BDFIM given in Table I, s_1 is in the range of 0.57 to 0.77. So, the asynchronous torques corresponding to the resistance $R_r/s_1$are relatively small and therefore can be neglected [19], [24]. Although the induction machine without presence of the rotor resistance cannot produce torque, the power conversion and the torque production will accomplish in BDFIM, even by neglecting the rotor resistance. In [20], it has been shown by ignoring the rotor resistance, the torque expression can be written similar to a conventional synchronous machine.

In light of foregoing, regardless of the resistance $R_r/s_1$and by applying delta-to-star transform to the rotor loop reactances in Fig. 1, the steady-state equivalent circuit of BDFIM turns into a fifth-order model, as shown in Fig. 2. For this model, the following expressions are obtained based on the inductances of BDFIM complete model [19]:

$$L_{l1}^{new} = L_{l1} + \frac{L_{1r}.L_{lr}}{L_{1r}+L_{2r}+L_{lr}}, L_{l2}^{\text{new}} = L_{l2} + \frac{L_{2r}.L_{lr}}{L_{1r}+L_{2r}+L_{lr}} L_{12} = -\frac{L_{1r}.L_{2r}}{L_{1r}+L_{2r}+L_{lr}}. \quad (3)$$

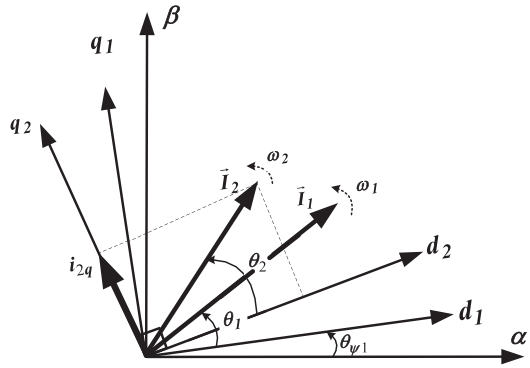

Fig. 3. Current vectors used in the equations and their interrelationships.

The two-axis dynamic fifth-order model of BDFIM is written as [19]

$$\vec{V_1} = R_1\vec{I_1} + \frac{d\vec{\psi_1}}{dt} + j\omega_1\vec{\psi_1} \quad (4)$$

$$\vec{V_2} = \vec{R}_2\vec{I_2} + \frac{d\vec{\psi_2}}{dt} + j\,\omega_2\vec{\psi_2} \quad (5)$$

$$\vec{\psi_1} = (L_{l1}^{\text{new}} + L_{12}).\,\vec{I_1} + L_{12}\vec{I_2^*} = L_p\vec{I_1} + L_{12}\vec{I_2^*} \quad (6)$$

$$\vec{\psi_2} = (L_{l2}^{\text{new}} + L_{12}).\,\vec{I_2} + L_{12}\vec{I_1^*} = L_s\vec{I_2} + L_{12}\vec{I_1^*}. \quad (7)$$

In deriving the two-axis voltage equations, we referred (4) and (5) to reference frames rotating at ω_1 and ω_2, respectively. This interpretation of reference frames has been reported in [17]. The electromagnetic torque of fifth-order model can be expressed as

$$T_e = -\frac{3}{2}N_r.\,L_{12}\text{Im}\left[\vec{I_1^*}\vec{I_2^*}\right]. \quad (8)$$

Equation (8) is derived by substituting (4) and (5) into space vector expression of total three-phase active input power**.**

III. PROPOSED CONTROL STRATEGY

A. MTPIA Control

The MTPIA strategy is obtained with minimization of CW current magnitude under the constant torque. Hence, the torque equation should be rewritten in terms of the CW current. For this purpose, (8) is written as follows:

$$T_e = \alpha(\psi_{1d}i_{2q} + \psi_{1q}i_{2d}) \quad (9)$$

where $\alpha = \frac{3}{2}(\frac{N_r.L_{12}}{L_p})$.

The PW flux orientation is achieved by aligning *d*-axis of the synchronous reference frame with the PW flux vector. The resultant d and *q*-axis PW flux components are

$$\psi_{1d} = \left|\vec{\psi_1}\right| \quad , \quad \psi_{1q} = 0. \quad (10)$$

From Fig. 3, one can see that $i_{2q} = |\vec{I_2}|\,\sin\theta_2$, and consequently, the MTPIA is written as

$$T_e/|\vec{I_2}| = \alpha\left|\vec{\psi_1}\right|\sin\theta_2. \quad (11)$$

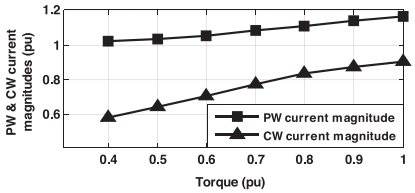

Fig. 4. PW and CW current magnitudes under MTPIA.

It is apparent that $T_e/|\vec{I}_2|$ will maximize when $\theta_2 = \pi/2$. In other words, for MTPIA realization, the CW d-axis current should be equal to zero. This criterion which leads to minimum inverter rating, has been also proved for cascaded doubly-fed induction machine [25], and for BDFRM [26], [27]. Fig. 4 presents the individual current magnitudes flowing in the BDFIM.

B. MTPTA Control

A desirable strategy for controlling the BDFIM is the maximum torque per total amperes of the machine. In this strategy, it is necessary to derive expressions for the torque and the total current magnitude based on the PW and the CW current angles. In the following, it is demonstrated how these equations are derived.

1) Derivation of Electromagnetic Torque: In this section, the procedure for deriving the torque formula used for MTPTA strategy is proposed. The basic expression of torque (8) can be manipulated into a variety of forms. Another form of torque is stated in terms of two-axis components of PW flux and current

$$T_e = \beta.(\psi_{1d} i_{1q} - \psi_{1q} i_{1d}) \tag{12}$$

where $\beta = \frac{3}{2} N_r$.

In FOC scheme, the PW flux orientation has been selected, therefore (9) and (12) can be written as

$$T_e = \alpha \left(\left|\vec{\psi}_1\right| \, i_{2q} \right) \tag{13}$$

$$T_e = \beta \left(\left|\vec{\psi}_1\right| \, i_{1q} \right) \tag{14}$$

Therefore, the torque can be controlled by the PW and the CW q-axis current, respectively. From Fig. 3, it can be seen that $i_{1q} = |\vec{I}_1| \sin\theta_1$ and $i_{2q} = |\vec{I}_2| \sin\theta_2$. So, (13) and (14) are rewritten as follows:

$$T_e = \alpha \left|\vec{\psi}_1\right| . \left|\vec{I}_2\right| \sin\theta_2$$

$$T_e = \beta \left|\vec{\psi}_1\right| . \left|\vec{I}_1\right| \sin\theta_1. \tag{15}$$

Substituting $\vec{I}_1 = |\vec{I}_1| \, e^{j\theta_1}$ and $\vec{I}_2 = |\vec{I}_2| \, e^{j\theta_2}$ into (8), and after a few manipulations, we can derive the following equation:

$$T_e = \gamma \left|\vec{I}_1\right| . \left|\vec{I}_2\right| \sin(\theta_1 + \theta_2) \tag{16}$$

where $\gamma = \beta . L_{12}$.

Comparing (15) and (16), (17) and (18) are, respectively, obtained for the PW and the CW current magnitudes

$$\left|\vec{I}_1\right| = \frac{\left|\vec{\psi}_1\right| \sin\theta_2}{L_p \sin(\theta_1 + \theta_2)} \tag{17}$$

$$\left|\vec{I}_2\right| = \frac{\left|\vec{\psi}_1\right| \sin\theta_1}{L_{12} \sin(\theta_1 + \theta_2)}. \tag{18}$$

Substituting (17) and (18) into (16), we have

$$T_e = \gamma \frac{\left|\vec{\psi}_1\right| \sin\theta_2}{L_p \sin(\theta_1 + \theta_2)} . \frac{\left|\vec{\psi}_1\right| \sin\theta_1}{L_{12} \sin(\theta_1 + \theta_2)} \sin(\theta_1 + \theta_2)$$

$$= \beta . \frac{\left|\vec{\psi}_1\right|^2 \sin\theta_1 . \sin\theta_2}{L_p \sin(\theta_1 + \theta_2)}. \tag{19}$$

2) Derivation of Total Current Magnitude: As mentioned earlier, to realize the MTPTA, the sum of the PW and the CW current magnitudes ($|\vec{I}_T|$) should be minimized for a given torque. Considering (17) and (18), the total current magnitude is defined as

$$\left|\vec{I}_T\right| = \left|\vec{I}_1\right| + \left|\vec{I}_2\right| = \frac{\left|\vec{\psi}_1\right| \sin\theta_2}{L_p \sin(\theta_1 + \theta_2)} + \frac{\left|\vec{\psi}_1\right| \sin\theta_1}{L_{12} \sin(\theta_1 + \theta_2)}. \tag{20}$$

The current angles are not independent due to flux and frame alignment conditions. In order to minimize (20), we need to find the relationship that exits between $\theta_1$and θ_2. In this regard, by (6) and (14)

$$\frac{i_{2q}}{i_{2d}} = \tan\theta_2 = \frac{T_e L_p}{\beta \left|\vec{\psi}_1\right| \left(\left|\vec{\psi}_1\right| - L_p i_{1d} \right)} \tag{21}$$

which can be simplified to give

$$i_{1d} = \frac{\beta \left|\vec{\psi}_1\right|^2 \tan\theta_2 - T_e L_p}{\beta \left|\vec{\psi}_1\right| L_p \tan\theta_2}. \tag{22}$$

Likewise, from (14) and (22)

$$\frac{i_{1q}}{i_{1d}} = \tan\theta_1 = \frac{T_e L_p \tan\theta_2}{\beta \left|\vec{\psi}_1\right|^2 \tan\theta_2 - T_e L_p}. \tag{23}$$

Equation (23) is the fundamental relationship that should exit between the current angles, and it is allows us to convert the expression for $|\vec{I}_T|$to be in one variable.

We can manipulate (20) as follows:

$$\left|\vec{I}_T\right| = \frac{\frac{|\vec{\psi}_1| L_{12} \tan\theta_2}{\cos\theta_1} + \frac{|\vec{\psi}_1| L_p \tan\theta_1}{\cos\theta_2}}{L_p L_{12} (\tan\theta_1 + \tan\theta_2)}. \tag{24}$$

Now, by knowing $\cos\theta_i = 1/(\sqrt{1 + \tan^2\theta_i})$, $(i = 1, 2)$ and substituting (23) into (24), an expression is achieved for $|\vec{I}_T|$ in terms of θ_2

$$\left|\vec{I}_T\right| = \frac{\sqrt{\left(\beta \left|\vec{\psi}_1\right|^2 \tan\theta_2 - T_e \, L_p\right)^2 + \left(T_e \, L_p \tan\theta_2\right)^2}}{\beta \, L_p \left|\vec{\psi}_1\right| \tan\theta_2}$$

$$+ \frac{L_p T_e \sqrt{1 + \tan^2\theta_2}}{\beta \, L_{12} \left|\vec{\psi}_1\right| \tan\theta_2}. \tag{25}$$

To obtain the minimum value of$|\vec{I}_T|$for a given torque, differentiate of (25) relative to $\tan\theta_2$ should be equal to zero. Due to

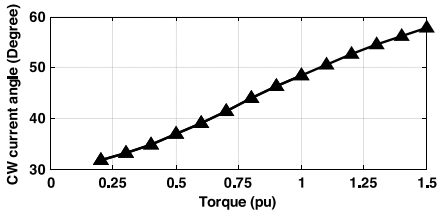

Fig. 5. CW current angles (θ_2) under MTPTA.

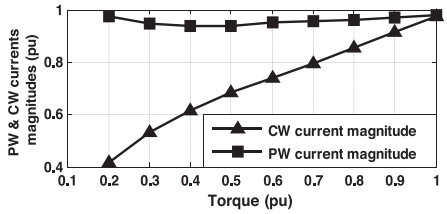

Fig. 6. PW and CW current magnitude components under MTPTA [according to (17) and (18)].

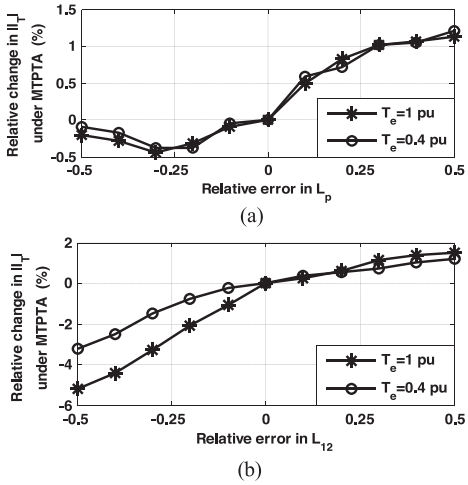

Fig. 7. Relative change in minimum value of total current magnitude against error in (a) L_p and (b) L_{12} (simulation).

the complexity of resultant derivative expression, there is no analytical solution for it. Therefore, the optimal value of θ_2 is calculated by using "fminserach" function and a numerical minimization approach is implemented in MATLAB. The CW current angles required for realization of MTPTA are shown in Fig. 5. The best fit to optimal CW current angle is constructed by curve fitting. For this purpose, the Curve Expert software, Version 1.3 is used. The following prototype curve is used for curve modeling of the CW current angle versus torque:

$$\theta_2 = d + \frac{a-d}{\left(1+(T_e/c)^b\right)^m}. \tag{26}$$

It has found that the following parameters give the best fit: $a = 30.31314$, $b = 2.92411$, $c = 0.45286$, $d = 96.63678$, and $m = 0.26947$. According to (26), the optimal CW current angle is determined for a given torque. As a result, the realization criterion of MTPTA is achieved as follows:

$$\tan\theta_2 = i_{2q}/i_{2d} \Rightarrow i_{2d}\tan\theta_2 - i_{2q} = 0. \tag{27}$$

Equation (27) indicates for realization of MTPTA, $i_{2d}\tan\theta_2 - i_{2q}$, which is chosen as the first control output, should be forced to zero. The MTPA control strategy is realized for an ideal induction machine as the stator current angle is $\pi/4$. For BDFIM, the CW current angles, which depend on the torque level, are however less or more than $\pi/4$. Fig. 6 shows the individual current magnitudes for different torques under MTPTA. This plot shows that the change in the total current is largely due to changes in the CW current magnitude.

It is obvious that (25) is dependent on having knowledge of L_p and L_{12}. The question then arises as to how accurately these parameters must be known. In order to determine this, a sensitivity analysis is carried out to determine the effect that inaccurate knowledge of L_p and L_{12} has on $|\vec{I}_T|$ under MTPTA. The results are plotted in Fig. 7. It can be seen that even though the minimum value of $|\vec{I}_T|$ is relatively sensitive to L_{12}, this value is insensitive to an error in L_p when it is in the range of $\pm 50\%$.

IV. Input–Output Feedback Linearization for BDFIM

In order to obtain the control inputs, the nonlinear control technique is applied to the BDFIM drive system This article does not develop the IOFL theory (see e.g., [28]), but shows directly its application on the BDFIM. Therefore, by choosing $x_1 = i_{1d}$, $x_2 = i_{1q}$, $x_3 = i_{2d}$, $x_4 = i_{2q}$, and $x_5 = \omega_r$ as state variables, $y = [y_1\ y_2]^T$ as output vector, and $u = [u_1\ u_2]^T$ as input vector, the fifth-order affine model is described by

$$\dot{X} = f(X) + g(X)U \tag{28}$$

with $X = [x_1\ x_2\ x_3\ x_4\ x_5]^T = [i_{1d}\ i_{1q}\ i_{2d}\ i_{2q}\ \omega_r]^T$, the equation shown at the bottom of this page
and

$$g(X) = [g_1\ g_2] = \frac{1}{\sigma . L_{12}} . \begin{bmatrix} 1 & 0 & -\frac{L_p}{L_{12}} & 0 & 0 \\ 0 & -1 & 0 & -\frac{L_p}{L_{12}} & 0 \end{bmatrix}^T$$

where $\sigma = 1 - (L_p . L_s / L_{12}^2)$ and $T_e = \frac{3}{2} N_r . L_{12} . (x_1 . x_4 + x_2 . x_3)$.

Choosing MTPTA strategy (27) and BDFIM torque as output variables, the tracking errors are introduced as

$$e = \begin{bmatrix} e_{y_1} \\ e_{y_2} \end{bmatrix} = \begin{bmatrix} y_1 - y_{1_{ref}} \\ y_2 - y_{2_{ref}} \end{bmatrix} = \begin{bmatrix} i_{2d}\tan\theta_2 - i_{2q} \\ T_e - T_{e,ref} \end{bmatrix} \tag{29}$$

Therefore, the error dynamics are defined as

$$\begin{bmatrix} \dot{e}_{y_1} \\ \dot{e}_{y_2} \end{bmatrix} = \begin{bmatrix} L_f y_1 \\ L_f y_2 \end{bmatrix} + \begin{bmatrix} L_{g1}y_1 & L_{g2}y_1 \\ L_{g1}y_2 & L_{g2}y_2 \end{bmatrix} . \begin{bmatrix} u_1 \\ u_2 \end{bmatrix} - \begin{bmatrix} 0 \\ \dot{y}_{2,ref} \end{bmatrix} \tag{30}$$

where $L_f y_i$ and $(i = 1, 2)$ are the directional (or Lie) derivative of state function $y(x) : R^n \to R$ along a vector field $f\ (x) =$

$[f_1(x),\ \ldots,\ f_n(x)]$

$$L_f y(x) = \sum_{i=1}^{n} \frac{\partial y(x)}{\partial x} f_i(x). \tag{31}$$

Choosing (32) as a Lyapunov function candidate, the control inputs are determined in such a manner that the asymptotically stable criterion is satisfied

$$V = \frac{1}{2} e^T e > 0. \tag{32}$$

Time derivative of the Lyapunov function is given by

$$\dot{V} = -e^T \Gamma\, e < 0 \tag{33}$$

where$\Gamma = \begin{bmatrix} c_{y_1} & 0 \\ 0 & c_{y_2} \end{bmatrix}$is a positive definite matrix.

Based on the above relations, the control inputs are obtained as

$$\begin{bmatrix} u_1 = V_{2d}^* \\ u_2 = V_{2q}^* \end{bmatrix} = \begin{bmatrix} \tan\theta_2 & -1 \\ x_4 - \frac{L_p}{L_{12}}.x_2 & -\left(x_3 + \frac{L_p}{L_{12}}.x_1\right) \end{bmatrix}^{-1}$$

$$\times \begin{bmatrix} \frac{\sigma.L_{12}^2}{L_p}.(\tan\theta_2.f_3 - f_4 + c_{y_1}e_1) \\ -\sigma.L_{12}.(x_4.f_1 + x_3.f_2 + x_2.f_3 + x_1.f_4) \\ -\frac{\sigma}{1.5.N_r}.(c_{y_2}e_2 - \dot{y}_{2,ref}) \end{bmatrix}. \tag{34}$$

Therefore, the error dynamics equations are

$$\dot{e}_{y_1} = -c_{y_1}.e_{y_1} \quad , \quad \dot{e}_{y_2} = -c_{y_2}.e_{y_2}\,. \tag{35}$$

These equations show that for positive c_{y1} and c_{y2}, e_{y1} and e_{y2} exponentially converge to zero. In order to achieve the acceptable performance, the controller coefficients are tuned in the simulation and the experiment. The control inputs of MTPIA are derived similar to the proposed procedure for MTPTA [see Appendix].

In order to study the sensitivity of the proposed controller (MTPTA-IOFL) to the motor parameters variation, relative change in $|\vec{I}_T|$ due to $k_1 = L_p/L_{12}$, $k_2 = \sigma L_{12}$ and $k_3 = L_s/L_{12}$ are shown in Fig. 8. According to (34), these coefficients perform key roles for the derived control inputs. The conclusion which can be achieved from these plots is that the controller is more sensitive to error in k_1 and k_3 compared to k_2. If the value of k_2 is known with the accuracy of $\pm 50\%$, the variation of $|\vec{I}_T|$ will not be too great. However, k_1 and k_3 need to be known to an accuracy of $\pm 20\%$.

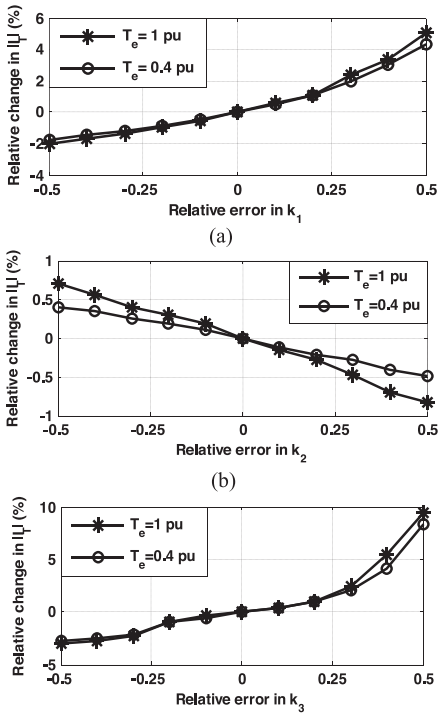

Fig. 8. Relative change in minimum value of total current magnitude against error in, (a) k_1, (b) k_2, and (c) k_3.

TABLE II
DC GENERATOR SPECIFICATIONS

Parameter	Value	Parameter	Value
Power (kW)	4.8	Rated current (A)	21
Rated voltage (V)	230	Rotor speed (rpm)	1500

V. RESULTS AND DISCUSSIONS

The performance of control strategies are studied in the simulation and the experimental tests at different operating conditions. The overall block diagram of the proposed drive system is illustrated in Fig. 9. Tables I and II show the specifications of BDFIM and dc generator, respectively. It should be noted that the natural speed is considered as base value for per-unit speed.

In order to evaluate the effectiveness of the proposed control scheme, some simulations are performed in MATLAB/Simulink. The MTPIA strategy is first considered. As shown in Figs. 10(a) and (b), the torque and the MTPIA strategy realization as two control objectives are satisfied using the

$$U = [u_1\ u_2]^T, f(X) = [f_1\ f_2\ f_3\ f_4\ f_5]^T$$

$$= \begin{bmatrix} \frac{1}{\sigma.L_{12}}\left(-\frac{L_s}{L_{12}}V_{1d} + \frac{R_1.L_s}{L_{12}}.x_1 + \omega_2.(L_s.x_4 - L_{12}.x_2) - R_2^p.x_3\right) \\ \frac{1}{\sigma.L_{12}}\left(-\frac{L_s}{L_{12}}V_{1q} + \frac{R_1.L_s}{L_{12}}.x_2 + \omega_2.(L_s.x_3 + L_{12}.x_1) + R_2^p.x_4 + \frac{\omega_1.L_s.|\vec{\psi}_1|}{L_{12}}\right) \\ \frac{1}{\sigma.L_{12}}\left(V_{1d} - R_1.x_1 + \omega_2.L_p.(x_2 - \frac{L_s}{L_{12}}.x_4) + \frac{R_2^p.L_p}{L_{12}}.x_3\right) \\ \frac{1}{\sigma.L_{12}}\left(-V_{1q} + R_1.x_2 + \omega_2.L_p.(x_1 + \frac{L_s}{L_{12}}.x_3) + \frac{R_2^p.L_p}{L_{12}}.x_4 + \omega_1.\left|\vec{\psi}_1\right|\right) \\ \frac{1}{J}(T_e - T_L - B.x_5) \end{bmatrix}$$

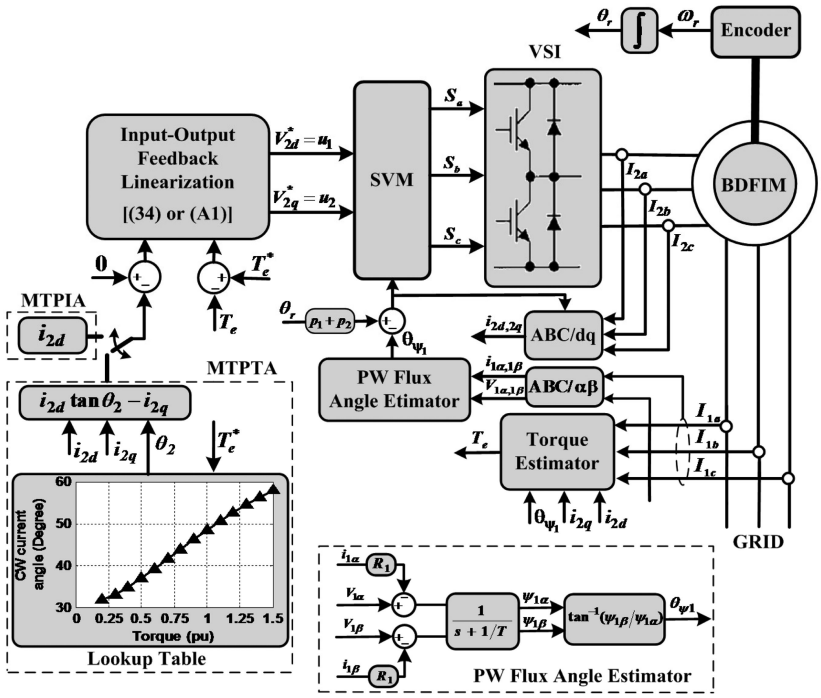

Fig. 9. Structural block diagram of BDFIM-based drive system.

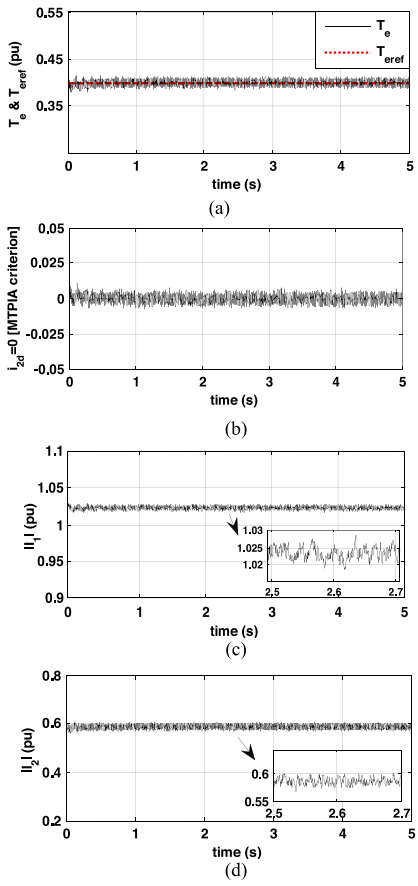

Fig. 10. Simulation results of MTPIA control strategy during steady-state operation. (a) Electromagnetic torque. (b) MTPIA realization criterion. (c) PW current magnitude. (d) CW current magnitude.

nonlinear controller. The CW d-axis current always fluctuates around zero which means that the MTPIA strategy is realized. The magnitude of stator currents are illustrated in Figs. 10(c) and (d), respectively. As observed in Fig. 11, along with the realization of MTPTA strategy, the electromagnetic torque properly tracks the repeating sequence of reference torque between 0.4 and 1 p.u. Fig. 11(c) and (d) shows that the PW and the CW current magnitudes change with respect to the torque command. It can be found that by realizing the MTPIA strategy, the CW current magnitude reduces in comparison with MTPTA one.

As shown in Figs. 10(d) and 11(d), for $T_e = 0.4$ p.u., the CW current magnitudes under MTPIA and MTPTA strategies are approximately 0.58 and 0.62 p.u., respectively. Referring to Fig. 11(c), the magnitude of PW current is 0.97 p.u., under the case of $T_e = 1$ p.u. This value which is almost equal to CW current [see Fig. 11(d)], is consistent with that obtained in Fig. 6.

It is shown in Fig. 11, by increasing the torque, the PW current magnitude is relatively constant but the CW current magnitude considerably increases. This result, which is confirmed through Fig. 6, is not unexpected since the CW current angle is larger than the PW current angle. Then, variations in the CW current magnitude will reflect more in the q-axis current. This current is responsible for the torque production; therefore it is the CW current that mostly changes with changing torque demands.

The practical evaluation of the actual system performance is fulfilled through a DSP-based prototype system. The experimental setup shown in Fig. 12 consists of a voltage source inverter with corresponding driver board, a sensor board, and a TMS320F28335 signal processor board designed with Texas Instrument Co. The rotor speed is measured by a 1024-pulse incremental encoder mounted on the BDFIM shaft. The stator

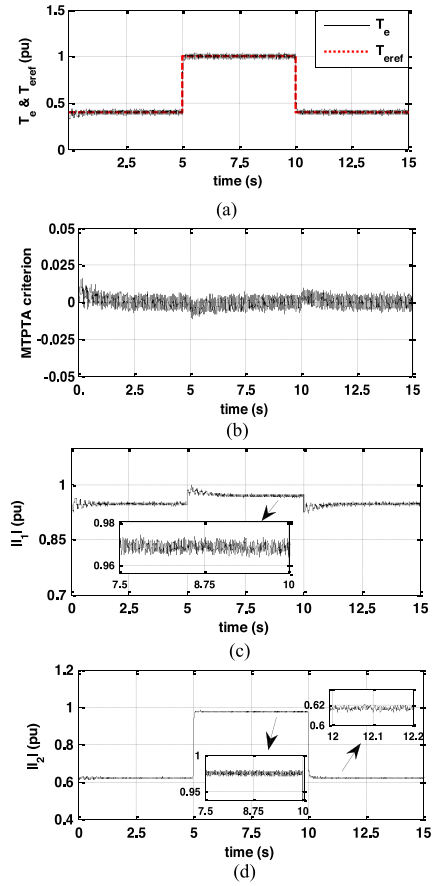

Fig. 11. Simulation results of MTPTA control strategy during transient operation. (a) Electromagnetic torque. (b) MTPTA realization criterion. (c) PW current magnitude. (d) CW current magnitude.

phase currents are measured using Hall-effect current sensors and the line-to-line voltages are detected by voltage sensors.

The performance of MTPIA and MTPTA control schemes are experimentally verified for steady-state and transient conditions by adopting the same objectives as the simulation results. As shown in Figs. 13 and 14, a close agreement is observed between the simulation and experimental results. Any difference can be explained because of using the reduced order model for simulation, magnetic saturation, and iron loss that are not taken into account for the BDFIM control scheme, etc. Fig. 14 illustrates how the magnitude of the PW and the CW currents change with torque variations. These results are consistent with Fig. 6 and similar to those already obtained in the simulation section. The high torque ripple appearing in Figs. 13(a) and 14(a) is due to the nested-loop rotor structure. Because the rotor is designed to couple two main harmonic field components, it produces a large space-harmonic distortion. This affects the machines operating behavior. The increased space harmonic distortion increases rotor leakage inductivity, which could be used beneficially to improve low voltage ride through performance [29]. The drawback of increased space harmonic is that it causes additional torque ripple in the BDFIM.

The performance of both MTPIA and MTPTA strategies are also evaluated at the same experiment for $T_e = 0.4$ p.u. In this

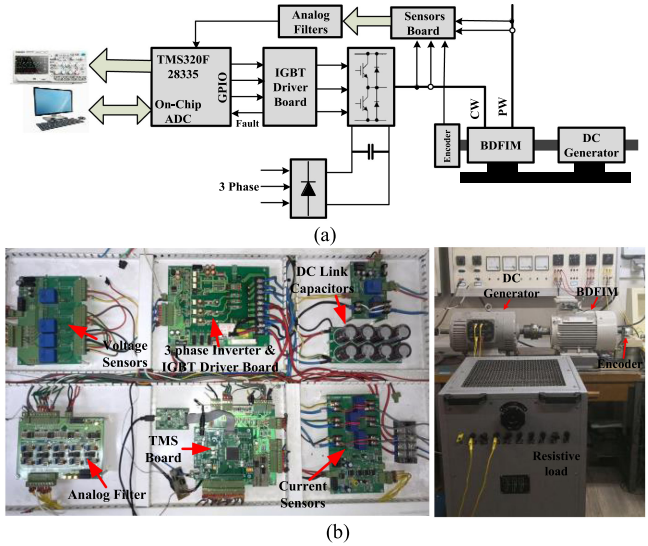

Fig. 12. Experimental setup. (a) Laboratory implementation block diagram. (b) BDFIM drive system hardware.

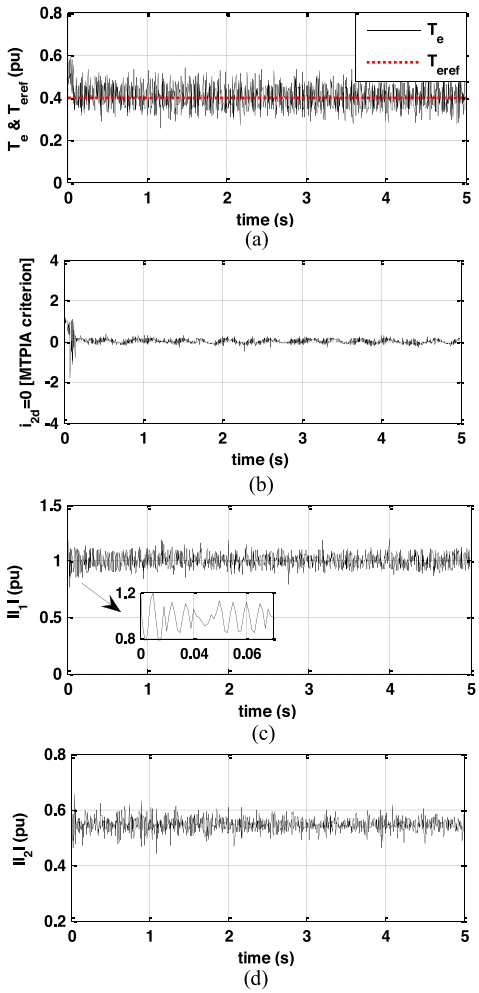

Fig. 13. Experimental results of MTPIA control strategy during steady-state operation. (a) Electromagnetic torque. (b) MTPIA realization criterion. (c) PW current magnitude. (d) CW current magnitude.

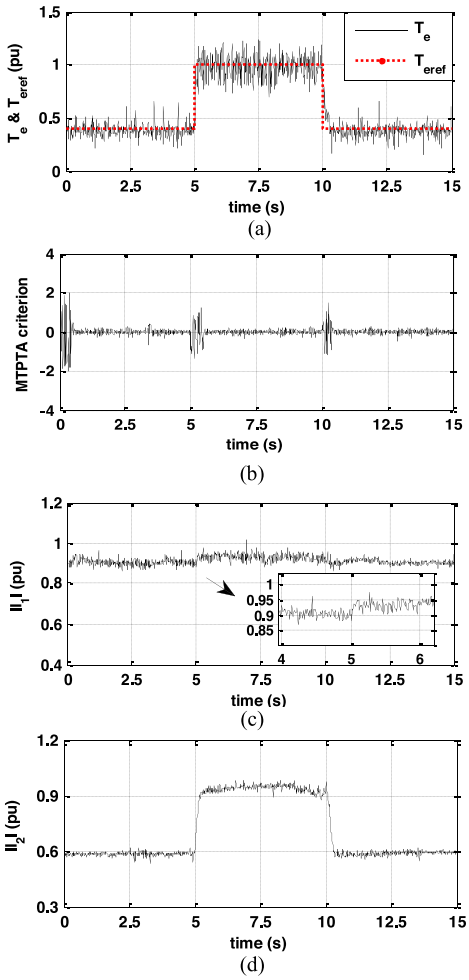

Fig. 14. Experimental results of MTPTA control strategy during transient operation. (a) Electromagnetic torque. (b) MTPTA realization criterion. (c) PW current magnitude. (d) CW current magnitude.

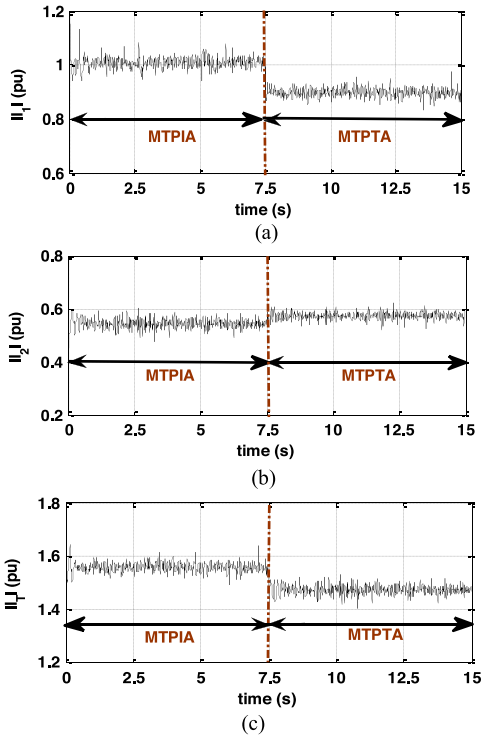

Fig. 15. Comparison of MTPIA and MTPTA performance. (a) PW current magnitude. (b) CW current magnitude. (c) Total current magnitude.

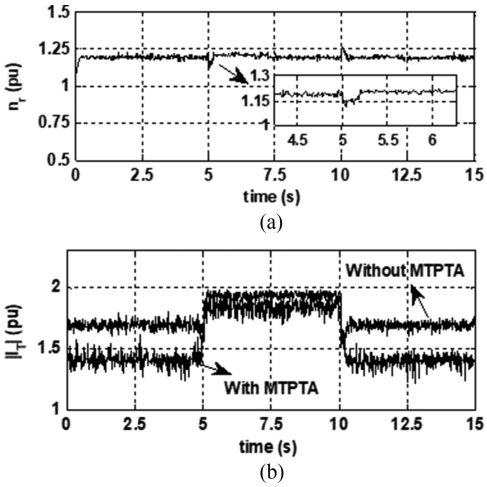

Fig. 16. Experimental results of BDFIM speed control. (a) Rotor speed. (b) Total current magnitude with and without MTPTA.

regard, the MTPIA strategy is firstly fulfilled by forcing the CW d-axis current to zero. Then, this strategy is removed and the MTPTA strategy is simultaneously applied to the BDFIM, as illustrated in Fig. 15. Even though the MTPTA strategy results in an increment on the magnitude of CW current, the sum of the PW and the CW current magnitudes decreases compared to MTPIA one.

An additional scenario is carried out to further evaluate the achievement of the MTPTA control strategy. Accordingly, the control strategy is compared to the conventional FOC with rated flux. In this condition, the BDFIM drive system is equipped with the closed-loop speed control and the error signal of speed with respect to the actual value is delivered to the PI controller. Torque command is then determined by speed loop controller output. The rotor speed is controlled at $n_r = 1.2$ p.u. [see Fig. 16(a)]. The load torque is first stepped up from 0.4 to 1 p.u. Then, the load torque is stepped down to 0.4 p.u. and, as a result, the BDFIM returns to its initial operating condition. The step change of load torque can be provided by connecting/disconnecting the dc generator field supply, which results in a sluggish response and time delay due to the large time constant of the dc generator excitation circuit. In order to avoid this, the load torque is standardly changed by connecting/disconnecting the load resistor. Fig. 16(b) shows the total current magnitude of the BDFIM with and without the proposed strategy. It can be seen that under the MTPTA control method, $|\vec{I}_T|$ considerably reduces in comparison with the constant flux method. The stator current waveforms under MTPTA, which is obtained from this experiment, are also plotted in Fig. 17. In order to clearly show the dynamic changes in both stator winding currents, the time interval is between 9.7 to 10.3 s.

In a similar way, the operation of BDFIM drive is evaluated under speed control with and without MTPIA control strategy. To do this, the rotor speed reference is set on 1.2 p.u., and $T_l =$

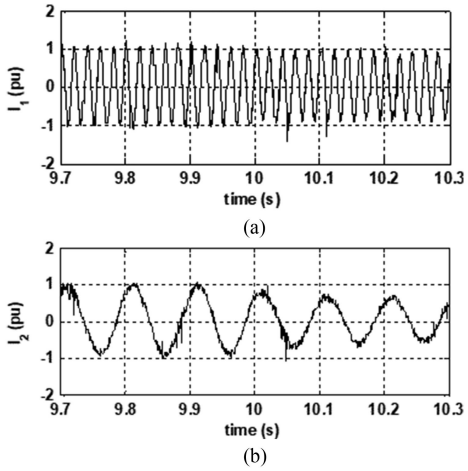

Fig. 17. Experimental PW/CW currents under MTPTA with speed control ($f_1 = 50$ Hz and $f_2 = 10$ Hz). (a) PW current. (b) CW current.

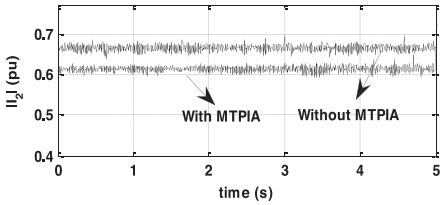

Fig. 18. CW current magnitude with and without MTPIA.

0.4 p.u. As observed in Fig. 18, by implementing the MTPIA, the CW current magnitude decreases about 8% in comparison with the FOC.

VI. Conclusion

In this article, a control strategy was proposed which maximizes the ratio of torque to total input currents flowing into the BDFIM stator windings. This strategy is essentially trying to share the current more evenly between the windings for a given torque. Due to the flux and frame alignment conditions, the PW and CW current angles are not independent. Accordingly, a fundamental relationship was obtained between these angles which allow us to derive the expression of total stator current magnitude in terms of CW current angle. The optimal angle which realizes the MTPTA control strategy was then calculated by using a numerical minimization procedure. Moreover, the MTPIA strategy was proposed and it was proven to minimize the CW current magnitude for a given torque, the CW current angle should be always constant. In the experiments, the proposed strategy was compared to the conventional FOC and it was shown that for load torque periodically changed between 0.4 and 1 p.u., the reduction of total current magnitude is nearly 12.23% and 4.15%, respectively.

Appendix

$$\begin{bmatrix} u_1 = V_{2d}^* \\ u_2 = V_{2q}^* \end{bmatrix} = \begin{bmatrix} 1 & 0 \\ x_4 - \frac{L_p}{L_{12}}.x_2 & -\left(x_3 + \frac{L_p}{L_{12}}.x_1\right) \end{bmatrix}^{-1} \times \begin{bmatrix} \frac{\sigma.L_{12}^2}{L_p}.(f_3 + c_{y_3}e_1) \\ -\sigma.L_{12}.(x_4.f_1 + x_3.f_2 + x_2.f_3 + x_1.f_4) \\ -\frac{\sigma}{1.5.N_r}.(c_{y_4}e_2 - \dot{y}_{2,ref}) \end{bmatrix} \quad \text{(A1)}$$

References

[1] A. K. Wallace, R. Spee, and H. K. Lauw, 'The potential of brushless doubly-fed machines for adjustable speed drives," in *Proc. Pulp Paper Ind. Tech. Conf.*, Jun. 18–22, 1990.

[2] J. Chen, W. Zhang, B. Chen, and Y. Ma, "Improved vector control of brushless doubly fed induction generator under unbalanced grid conditions for offshore wind power generation," *IEEE Trans. Energy Convers.*, vol. 31, no. 1, pp. 293–302, Mar. 2016.

[3] E. Abdi *et al.*, "Performance analysis and testing of a 250 kW medium-speed brushless doubly-fed induction generator," *IET Renew. Power Gener.*, vol. 7, no. 6, pp. 631–638, Apr. 2013.

[4] D. Zhang, Y. Chen, J. Su, and Y. Kang, "Dual-mode control for brushless doubly fed induction generation system based on control-winding-current orientation," *IEEE J. Emerg. Sel. Topics Power Electron.*, to be published.

[5] J. Yang *et al.*, "Sensorless control of brushless doubly fed induction machine using a control winding current MRAS observer," *IEEE Trans. Ind. Electron.*, vol. 66, no. 1, pp. 728–738, Jan. 2019.

[6] N. Patin, E. Monmasson, and J. P. Louis, "Analysis and Control of a cascaded doubly-fed induction generator," in *Proc. IEEE Ind. Electron. Soc. Conf.*, Nov. 6–10, 2005.

[7] Y. Liu, W. Xu, J. Zhu, and F. Blaabjerg, " Sensorless Control of standalone brushless doubly-fed induction generator feeding unbalanced loads in ship shaft power generation system," *IEEE Trans. Ind. Electron.*, vol. 66, no. 1, pp. 739–749, May 2018.

[8] J. Poza, E. Oyarbide, I. Sarasola, and M. Rodriguez, "Vector control design and experimental evaluation for the brushless doubly-fed machine," *IET Elect. Power Appl.*, vol. 3, no. 4, pp. 247–256, Jul. 2009.

[9] R. Sadeghi, S. M. Madani, and M. Ataei, "A new smooth Synchronization of brushless doubly-fed induction generator by applying a proposed machine model," *IEEE Trans. Sustain. Energy*, vol. 9, no. 1, pp. 371–380, Jan. 2018.

[10] G. Zhang *et al.*, "A robust control scheme based on ISMC for the brushless doubly fed induction machine," *IEEE Trans. Power Electron.*, vol. 33, no. 4, pp. 3129–3140, Apr. 2018.

[11] C. Lascu, S. Jafarzadeh, S. M. Fadali, and F. Blaabjerg, "Direct torque control with feedback linearization for induction motor drives," *IEEE Trans. Power Electron.*, vol. 32, no. 3, pp. 2072–2080, Mar. 2017.

[12] A. Khazaee, H. Abootorabi Zarchi, and G. R. Arab Markadeh, "Real-time maximum torque per ampere control of brushless DC motor drive with minimum torque ripple," *IEEE Trans. Power Electron.*, vol. 35, no. 2, pp. 1194–1199, Feb. 2020.

[13] H. R. Mosaddegh Hesar, H. Abootorabi Zarchi, and M. Ayaz Khoshhava, "Online maximum torque per ampere control for induction motor drives considering iron loss using input–output feedback linearization," *IET Elect. Power Appl.*, vol. 13, no. 12, pp. 2113–2120, Dec. 2019.

[14] F. J. Lin, M. Huang, S. Chen, and C. Hsu, "Intelligent maximum torque per ampere tracking control of synchronous reluctance motor using recurrent Legendre fuzzy neural network," *IEEE Trans. Power Electron.*, vol. 34, no. 12, pp. 12080–12094, Dec. 2019.

[15] A. Shinohara, Y. Inoue, S. Morimoto, and M. Sanada, "Direct calculation method of reference flux linkage for maximum torque per ampere control in DTC-based IPMSM drives," *IEEE Trans. Power Electron.*, vol. 32, no. 3, pp. 2114–2122, Mar. 2017.

[16] B. V. Gorti, G. C. Alexander, R. Spee, and A. K. Wallace, "Microcontroller based efficiency maximization for a brushless doubly-fed machine pump drive," in *Proc. Int. Conf. Ind. Automat. Control*, Jan. 5–7, 1995.

[17] R. E. Betz and M. G. Jovanovic, "Introduction to the space vector modelling of the brushless doubly-fed reluctance machine," *Elect. Power Compon. Syst.*, vol. 31, no. 8, pp. 729–755, Jun. 2003.

[18] H. Mosaddegh, H. A. Zarchi and G. Arab Markadeh, "Stator flux oriented control of brushless doubly fed induction motor drives based on maximum torque per total ampere strategy," in *Proc. Int. Power Electron., Drive Syst. Technol. Conf.*, Feb. 12–14, 2019.

[19] S. Tohidi, "Analysis and simplified modelling of brushless doubly-fed induction machine in synchronous mode of operation," *IET Elect. Power Appl.*, vol. 10, no. 2, pp. 110–116, Feb. 2016.

[20] R. A. McMahon, P. C. Roberts, X. Wang, and P.J. Tavner, "Performance of BDFM as generator and motor," *IEE Elect. Power Appl.*, vol. 153, no. 2, pp. 289–299, Mar. 2006.

[21] A. C. F. Wiiliamson, and A. K. Wallace, "Generalised theory of the brushless doubly-fed machine. Part I: Analysis," *IEE Elect. Power Appl.*, vol. 144, no. 2, pp. 111–122, Mar. 1997.
[22] R. Li, A. K. Wallace, and R. Spee, "Dynamic simulation of brushless doubly-fed machines," *IEEE Trans. Energy Convers.*, vol. 6, no. 3, pp. 445–452, Sep. 1991.
[23] R. Li, R. Spk, A. K. Wallace, and G. C. Alexander, "Synchronous drive performance of brushless doubly-fed motors," *IEEE Trans. Ind. Appl.*, vol. 30, no. 4, pp. 963–970, Jul. 1994.
[24] Y. Liu, W. Xu, G. Zhi, and J. Zhang, "Performance analysis of a stand-alone brushless doubly-fed induction generator using a new t-type steady-state model," *J. Power Electron.*, vol. 17, no. 4, pp. 1027–1036, Jul. 2017.
[25] B. Hopfensperger, D. J. Atkinson, and R. A. Lakin, "Combined Magnetising flux oriented control of the cascaded doubly-fed induction machine," *IEE Elect. Power Appl*., vol. 148, no. 4, pp. 354–362, Jul. 2001.
[26] M. G. Mousa, S. M. Allam, and E. M. Rashad, "Maximum power extraction under different vector-control schemes and grid-synchronization strategy of a wind-driven brushless doubly-fed reluctance generator," *ISA Trans*., vol. 72, pp. 287–297, Jan. 2018.
[27] S. Ademi and M. G. Jovanovic, "Maximum torque per inverter ampere control of brushless doubly-fed reluctance generators for wind turbines," *Int. Symp. Power Electron., Elect. Drives, Automat. Motion*, Ischia, Italy, Jun. 18–20, 2014.
[28] J. E. Slotine and W. Li, in *Application Nonlinear Control.* Englewood Cliffs, NJ, USA: Prentice-Hall, 1991.
[29] T. D. Strous, X. Wang, H. Polinder, and J. A. Ferreira, "Brushless doubly-fed induction machines: Torque ripple," in *Proc. Int. Elect. Mach. Drives Conf.*, May 10–13, 2015.

Hamidreza Mosaddegh Hesar received the B.Sc. and M.Sc. degrees in 2011 and 2014, respectively, from the Ferdowsi University of Mashhad, Iran, where he is currently working toward the Ph.D. degree.

His current interests and activities include control of high-performance drives, nonlinear control, and modeling of electrical machines.

Hossein Abootorabi Zarchi received the M.S. and Ph.D. degrees from the Isfahan University of Technology, Isfahan, Iran, in 2004 and 2010, respectively.

From May 2009 to February 2010, he was a Visiting Ph.D. Student with the Control and Automation Group, Denmark Technical University, Denmark. He is currently an Assistant Professor with the Department of Electrical Engineering, Ferdowsi University of Mashhad, Mashhad, Iran. His research interests include electrical machines, applied nonlinear control in electrical drives, and renewable energies.

Gholamreza Arab Markadeh received the B.Sc., M.Sc., and Ph.D. degrees in electrical engineering from the Isfahan University of Technology, Isfahan, Iran, in 1996, 1998, and 2005, respectively.

He is currently an Associate Professor with the Faculty of Engineering, Shahrekord University. His research interests include nonlinear control, power electronics, and variable-speed drives.

Dr. Markadeh is the Editor-in-Chief of *Journal of Dam and Hydroelectric Powerplant*. He was the recipient of the IEEE Industrial Electronics Society IECON'04 Best Paper Presentation Award in 2004.